



Mechanism and process of methylene blue degradation by manganese oxides under microwave irradiation



Xiaoyu Wang^a, Lefu Mei^a, Xuebing Xing^a, Libing Liao^{a,*}, Guocheng Lv^{a,*}, Zhaohui Li^{a,b}, Limei Wu^a

^a School of Material Sciences and Technology, China University of Geosciences, Beijing 100083, China

^b Geosciences Department, University of Wisconsin – Parkside, Kenosha, WI 53141-2000, USA

ARTICLE INFO

Article history:

Received 21 February 2014

Received in revised form 29 April 2014

Accepted 5 May 2014

Available online 22 May 2014

Keywords:

Microwave irradiation

Manganese oxides

Catalytic oxidation

Methylene blue

ABSTRACT

Numerous studies have been conducted on the removal of dyes from wastewater, although fewer were focused on the reactions under the influence of microwave irradiation (MI). In this paper, degradation of methylene blue (MB) in simulated wastewater by manganese oxides (MOs) under MI was investigated. A significant increase in MB removal efficiency by akhtenskite or birnessite was observed in the presence of MI. After 30 min MI, the MB removal by birnessite was 230 mg/g, in comparison to only 27 mg/g in the absence of MI. The kinetics of MB removal by MOs under MI followed the pseudo-first-order kinetic model well with rate constants of 0.005 and 0.04 min⁻¹ for akhtenskite and birnessite, respectively. In contrast, the rate constants were only 0.0006 and 0.0007 min⁻¹ for MB removal by akhtenskite and birnessite in the absence of MI. Results of XPS and LC–MS showed cyclic redox processes responsible for the step-wise degradation from MB to C₁₄H₁₃N₂OS, C₁₃H₁₁N₂OS, C₁₂H₈NO₂S, C₁₂H₉N₂OS, and eventually to smaller molecules. As akhtenskite and birnessite had no electric dipole moment in their crystal structure, it was deduced that stronger MI effect on MB removal by birnessite could be attributed to the larger spin dipole moment of the central manganese ion in octahedra.

© 2014 Elsevier B.V. All rights reserved.

1. Introduction

Recently, microwave irradiation (MI) to increase the efficiency of contaminant degradation is becoming increasingly important in wastewater treatment [1–3]. For example: a ClO₂–CuO_x/Al₂O₃ catalytic oxidation system could significantly enhance the removal of phenol under MI and the reaction fitted to the pseudo-first-order kinetic well [4]. NiFe₂O₄ could also gain a promising application in treatment of various dyestuff wastewaters under MI [5]. The removal of phenol by CoFe₂O₄ was significantly enhanced under MI with CoFe₂O₄ acting as a microwave catalyst [6]. NiFe₂O₄ and CoFe₂O₄ are ferrites which have excellent microwave adsorption to be used in magnetic and electronic products [7]. However, most of the previous studies on microwave adsorbents were focused on ferrites for the applications in electronic and magnetic fields [8–11]. In addition, previous studies of microwave catalytic oxidation were centered on the removal efficiency and physico-chemical conditions to achieve higher efficiency [12]. Few involved in discussion

on the reaction mechanism and the effect of structure details on catalytic properties.

Microwave catalysts are good microwave adsorbents. Their catalytic properties depend not only on chemical constituents, but also on grain size, lattice distortion, ion occupation, and electron configuration. Therefore, investigating the reaction mechanism, reaction process, and relationship between structural properties and degradation efficiency may present a great opportunity for the best selection of new microwave catalysts and microwave catalytic oxidation in environmental fields.

Manganese oxides (MOs) are excellent microwave adsorbents, which may play a potential role in organic pollutants removal. MOs are mainly constituted by [MnO₆] octahedra with tunnel or layered structure and are classified as pyrolusite–ramsdellite family with (1 × *n*) tunnel structure, hollandite–romanechite family with (2 × *n*) tunnel structure, todorokite family with (3 × *n*) tunnel structure, and birnessite family with (1 × ∞) layered structure [13,14]. MOs can produce “hotspot” under MI [15,16] and present an excellent oxidation capacity for the removal of organic macromolecules [17,18].

In this study, we reported a new approach that combines the use of MOs with MI for wastewater treatment using methylene blue (MB) as the example of contaminants. The focus of the

* Corresponding author. Tel.: +86 10 82320151.

E-mail addresses: lbiliao@cugb.edu.cn (L. Liao), guochenglv@cugb.edu.cn (G. Lv).

study was on elucidating structure characterization and oxidation mechanism, characterizing reaction products, and establishing relationship between degradation efficiency and intrinsic structural properties of the MOs.

2. Materials and methods

2.1. Experimental materials

KMnO₄, NaOH, MnCl₂·4H₂O, MB, and distilled water were purchased from Beijing Chemical Works. MB, also called 3,7-bis(dimethylamino)-phenothiazin-5-ium chloride, is a heterocyclic aromatic chemical compound with a molecular formula of C₁₆H₁₈N₃SCl and molar mass of 319.85 g/mol (284.35 g/mol in solution due to dissociation of Cl[−]). At room temperature it appears as a solid, odorless, dark green powder that yields a blue solution when dissolved in water. It is soluble in water (4 g/100 mL) and ethanol (1.5 g/100 mL) and insoluble in ether [19,20]. It is a typical dye in wastewater that leads to pollution of environment. Akhtenskite was obtained from Beijing Kang Puhui Technology Co., Ltd. while birnessite was synthesized according to the method by Feng et al. [21].

2.2. Methods of analyses

The crystal structures of MOs were characterized by X-ray diffraction (XRD) analysis under the following conditions: CuKα radiation at 40 kV and 100 mA, scanning speed at 8°/min, and 0.02°/step. The elemental compositions of MOs were determined by X-ray fluorescence spectrometry (XRF, Beijing North Early Microstructure Analysis and Test Center Co., Ltd.). The visible spectra of products from 500 to 700 nm were collected using an ultraviolet–visible spectroscopy (UV–vis, Beijing North Temple Instrument Technology Co., Ltd.) with an optical bandwidth of 2.0 nm, a response time of 0.2 s, medium scanning speed at an interval of 1 nm. The surface valence of MOs before and after MI was determined by X-ray photoelectron spectroscopy (XPS, Thermo Scientific Co., Ltd.) under a CuKα radiation, a power of 150 W, and a background pressure of 6.5×10^{-10} mbar. The molecular weight of the products was identified using HPLC–mass spectrometer (LC–MS, Thermo Scientific) and their molecular formulae were calculated using high resolution search (Thermo Scientific).

2.3. Microwave irradiation

A stock MB solution (500 mg/L) in distilled water was prepared and allowed to stand overnight. In batch experiments, 0.1 g of solid and 50 mL of MB stock solution were added into a glass beaker (100 mL). While, in the research of identifying the reaction pathway, 50 mL of MB (100 mg/L) and 0.1 g of birnessite were mixed in a glass beaker. Then the mixture was placed into a microwave reactor under a microwave power of 400 W. After MI, the slurry was cooled and centrifuged for 5 min at 6000 rpm. At the end of the process, a 10 mL aliquot of the supernatant was transferred and filtered with syringe-type filter to a 50-mL colorimetric tube for UV–vis analyses. All experiments were run in duplicates.

3. Results and discussion

3.1. Characterization of MOs structure

Akhtenskite had a space group of P6₃/mmc with $a = 2.8$ Å, $b = 2.8$ Å, $c = 4.45$ Å, $Z = 1$. It shows a NiAs type structure with the [MnO₆] octahedra in hexagonal close-packing [22]. The diffraction peaks of akhtenskite matched with those in the PDF card well. The

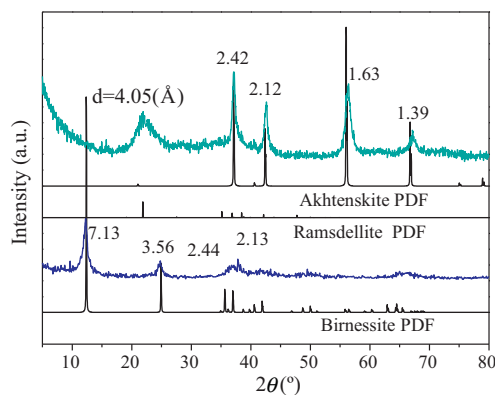


Fig. 1. XRD patterns of manganese oxides.

4.05 Å peak for akhtenskite should be very weak. Thus, the substantial higher peak at 4.05 Å was attributed to the (1 1 0) peak of ramsdellite [23]. Therefore, this MO was characterized as an akhtenskite with minor ramsdellite (Fig. 1). The birnessite-type MO, synthesized using the method of Feng et al. [21] had a space group of C2/m and unit cell parameters of $a = 5.175$ Å, $b = 2.849$ Å, $c = 7.338$ Å, $Z = 1$. Natural birnessite has good adsorption and cation-exchange properties [24] with a fine laminated texture. The ideal structure of birnessite consisted of [Mn(III)O₆] octahedra and [Mn(IV)O₆] octahedra, with one [Mn(III)O₆] octahedral chain inserted in two [Mn(IV)O₆] octahedral chains, and the negative charge was balanced by the interlayer ions [25,26]. Besides, the actually structure of birnessite usually contains little Mn(II) as the residue after synthesis based on the mechanism of adsorption of Mn(II) [27].

The chemical formulae determined by XRF were (Na, Al, K)_{0.03}Mn₂O₄ and (Na, K, Al)_{0.49}Mn₂O₄·0.62(H₂O) for akhtenskite and birnessite, respectively. Due to the higher large-cation content, it is anticipated that birnessite had a much higher fraction of Mn(III) in the lattice than akhtenskite.

3.2. Efficiencies and kinetics

In the absence of MO, the removal efficiency of MB by MI was almost 0% (Fig. 2a). In the presence of MO and absence of MI, the MB removal efficiency was approximately 10% after 30 min of reaction. A higher removal efficiency was achieved using birnessite compared to akhtenskite. This could be attributed to the surface charge of birnessite. Because of the replacement of Mn(III) for Mn(IV), the surface of birnessite was more negatively charged than that of akhtenskite. Therefore, the positively charged MB could be more easily adsorbed on the surface of birnessite. Similarly, an enhanced adsorption of ciprofloxacin on birnessite was noticed when ciprofloxacin was in a cationic form [24].

The MB removal efficiency increased to approximately 40% (removal amount of 98 mg/g) and 98% (removal amount of 230 mg/g) by akhtenskite and birnessite after 30 min MI, respectively (Fig. 2a), compared to the removal efficiency of approximately 9.8 and 10.9% by akhtenskite and birnessite in the absence of MI. These corresponded to an increase by a factor of 4 and 9, respectively. Similarly, the amounts of MB removal by akhtenskite and birnessite after 30 min MI increased from 25 to 98 and from 27 to 230 mg/g, respectively. As the removal efficiency was approximately 0% by MI in the absence of MO, it demonstrated that the residual oxygen in air was nonreactive with MB under MI. The significant increase of MB removal by MOs under MI suggested that MOs acted as oxidants and both akhtenskite and birnessite had an excellent response to MI. This approach was also obviously better than the methods of physical adsorption (maximum of 27 mg/g) or photochemical catalytic oxidation (maximum of 172.4 mg/g) [28].

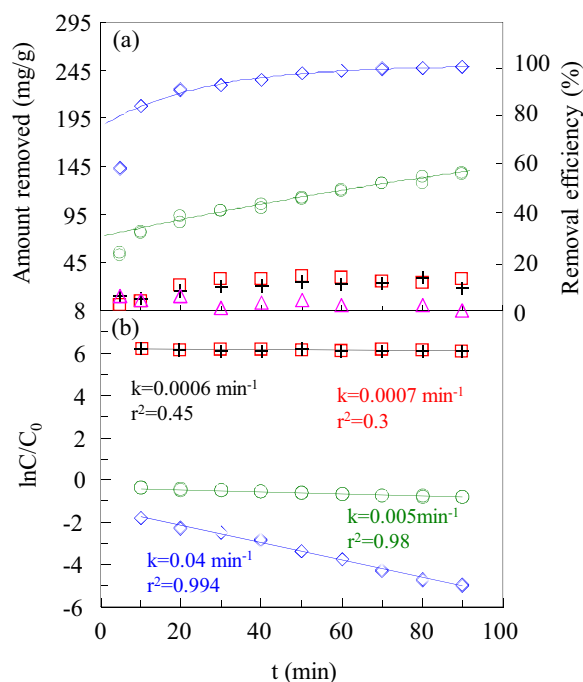


Fig. 2. Kinetics of MB removal by MOs in the presence or absence of MI. \diamond ; \circ ; \square ; \triangle ; and \blacktriangle were in systems of: MI/birnessite/MB; MI/akhtenskite/MB; birnessite/MB; akhtenskite/MB; and MI/MB (pH = neutral, $C_0 = 500 \text{ mg/L}$, temperature = $308 \pm 2 \text{ K}$ and amount of MO = 0.1 g).

MI could increase the surface reactivity of MOs and the temperature could rise to approximately 1378 K on MO surfaces [29], resulting in an accelerated MB removal. On the other hand, dissolved Mn(II) could be quickly oxidized by O_2 at high temperature which could contribute to the cyclic oxidation and reduction processes for regeneration of MOs and removal of MB. These results are in good agreements with previous study on the removal of PCB77 by MOs [18].

The kinetics of MB removal by akhtenskite and birnessite under MI fitted to the pseudo-first-order kinetic model well with rate constants of 0.005 and 0.04 min^{-1} and r^2 values of 0.98 and 0.994 , respectively (Fig. 2b), which were greater than the critical value r^2 of 0.95 previously determined [30]. In comparison, the rate constants of MB removal were only 0.0006 and 0.0007 min^{-1} by akhtenskite and birnessite in the absence of MI. An extrapolation for actual removal amount based on pseudo-first-order kinetic model showed that the theoretical and actual values matched well except at the beginning of reaction (Fig. 2a). This could be attributed to the rising temperature during the initial 10 min, which lead to a lower actual value than the theoretical one.

3.3. Reaction process and mechanism

The electron binding energy of $\text{Mn}2p_{3/2}$ for birnessite was determined by XPS after each treatment. The initial electron binding energy of $\text{Mn}2p_{3/2}$ in birnessite was 642.25 eV (Fig. 3a) [31]. While, a significant increase in electron binding energy of $\text{Mn}2p_{3/2}$ was found after 30 min MI (Fig. 3b). It declined to 642.12 eV after in contact with MB oxidation (or Mn(VI) reduction) (Fig. 3c) and increased after MI once again (Fig. 3d). As higher electron binding energy indicated higher oxidizability of Mn and lower electron binding energy indicated lower oxidizability, it was deduced that the average oxidizability of birnessite could be increased under MI and declined after MB oxidation, which suggested more Mn(IV) in birnessite could be achieved after MI. The multi-component spectral fitting of the peak $\text{Mn}2p_{3/2}$ was performed to detect the distribution of

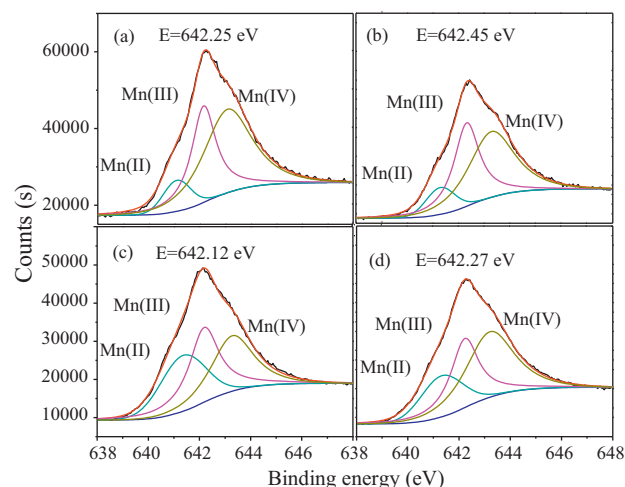


Fig. 3. XPS of raw birnessite (a), birnessite under MI (b), birnessite under MI + MB (c), birnessite under a second MI based on c (d).

various valence states of Mn on the surface of birnessite. Calculation showed that massive Mn(IV), Mn(III) and little Mn(II) were found on the surface of birnessite. The initial proportions of Mn(IV), Mn(III) and Mn(II) were 47.3 , 30.5 and 22.6% . After MI, the proportions of Mn(IV) and Mn(III) increased to 48.7 and 42.3% respectively. They declined to 32.4 and 36.8% after MB oxidation reaction and increased once again after a second MI (Table 1). An obvious cyclic trend was found with the valence of Mn increased under MI and decreased after reaction with MB. The oxidation reaction of Mn(II) was slow under normal conditions. However, dissolved Mn(II) could quickly be oxidized by O_2 under MI. Thus, MI could provide a high temperature environment and accelerate the sustainable cyclic redox reaction processes until complete removal of MB.

Fig. 4 presents the UV–vis spectra in the range of 500 – 700 nm of MB (initial at 100 mg/L) under MI and those of reaction products with 0.1 g birnessite under varying MI time using a microwave power of 400 W for 2 – 90 min . The maximum absorbance peak of MB in aqueous solution under MI was at 665 nm , according to a previous study [32]. Absorbance peaks of the products blue-shifted to 618 , 600 , 588 , and 562 nm as the MI time prolonged (Fig. 4). The products after MB degradation by thin layers of birnessite were Azure A, Azure B, Azure C, and thionin and the peaks at 618 and 600 nm were very close to the maximum absorbance peak of Azure C and thionin [33,34]. Thus, the MB degradation products were further confirmed by LC–MS for samples after 2 , 10 , and 60 min of MI, respectively (Fig. 5). The molecular weight of MB and its degradation intermediates were 284.3 , 257.1 , 243.1 , 230.0 , and 229.0 g/mol , corresponding to the molecular formulae of MB, $\text{C}_{14}\text{H}_{13}\text{N}_2\text{O}_5$, $\text{C}_{13}\text{H}_{11}\text{N}_2\text{O}_5$, $\text{C}_{12}\text{H}_8\text{NO}_2\text{S}$ and $\text{C}_{12}\text{H}_9\text{N}_2\text{O}_5$ using high resolution search. Among them, $\text{C}_{14}\text{H}_{13}\text{N}_2\text{O}_5$, $\text{C}_{13}\text{H}_{11}\text{N}_2\text{O}_5$, $\text{C}_{12}\text{H}_8\text{NO}_2\text{S}$ and $\text{C}_{12}\text{H}_9\text{N}_2\text{O}_5$ were just equal to the products after oxidation of $\text{C}_{14}\text{H}_{14}\text{N}_3\text{S}$ (Azure A), $\text{C}_{13}\text{H}_{12}\text{N}_3\text{S}$ (Azure C) and $\text{C}_{12}\text{H}_{10}\text{N}_3\text{S}$ (Thionin). It was speculated that the initial degradation intermediates were Azure A, Azure C, and thionin, and they were quickly oxidized by O_2 and/or Mn(VI) under high temperature to

Table 1
Results of XPS analysis.

	Manganese distribution		
	Mn(II) (%)	Mn(III) (%)	Mn(IV) (%)
Birnessite	22.6	30.6	47.3
Birnessite/MI	9.2	42.1	48.8
Birnessite/MI + MB	30.8	36.8	32.4
Birnessite/MI + MB + MI	21.8	37.1	41.1

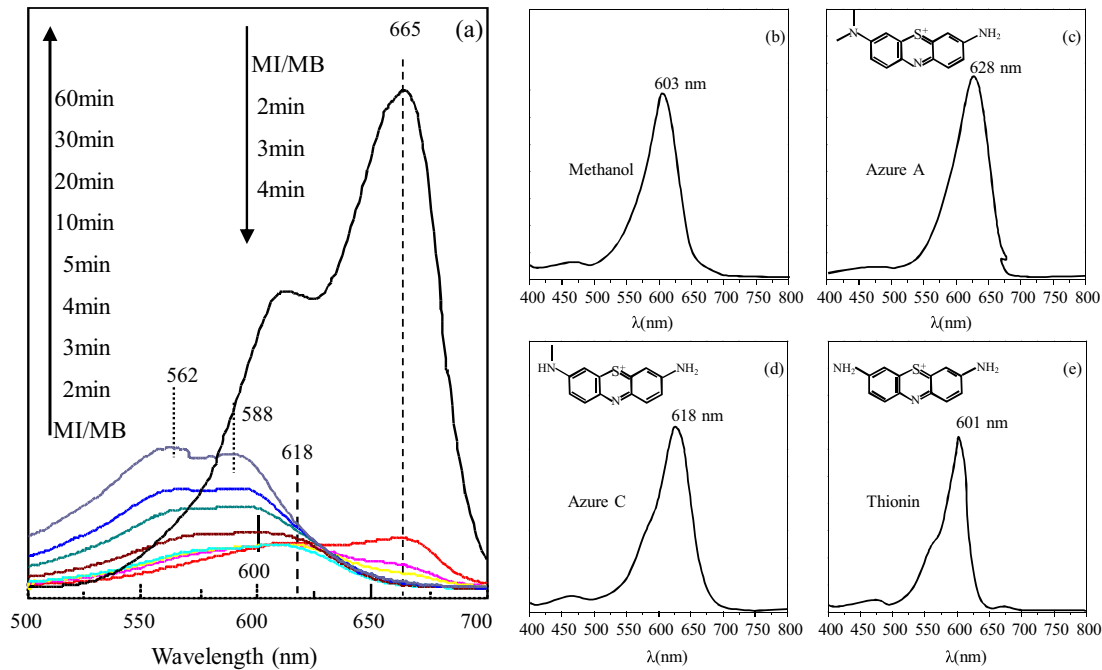


Fig. 4. UV-vis of MB under MI and products by birnessite after different MI time (a), compared to: (b) Methanol, (c) Azure A, (d) Azure C and (e) Thionin, dissolved in Methanol. —: MI/MB; —: 2 min; —: 3 min; —: 4 min; —: 5 min; —: 10 min; —: 20 min; —: 30 min; —: 60 min (pH = neutral, $C_0 = 100$ mg/L, temperature = 308 ± 2 K and amount of manganese oxide = 0.1 g).

$C_{14}H_{13}N_2OS$, $C_{13}H_{11}N_2OS$, $C_{12}H_8NO_2S$, $C_{12}H_9N_2OS$, and eventually to smaller molecules.

MOs can be used as microwave absorbents which will generate “hotspots” at temperature approximately 1378 K, resulting in the ability to accelerate the oxidative removal of MB [35,36]. Significant difference of catalytic ability between akhtenskite and birnessite correlates with the crystal structure closely. Understanding this difference requires a close look at the two-sided connection between the electric dipole moment of $[MnO_6]$ octahedra and the spin magnetic moment of central Mn. Considering the Jahn–Teller

Table 2
Calculation of lattice distortion.

Bond length distortion ($\Delta \times 10^3$)		
d	$\Sigma[(d_i - d_m)/d_m]^2$	$\Delta \times 10^3$
Akhtenskite		
1.9502	4.67×10^{-9}	2.34×10^{-9}
1.9502	4.67×10^{-9}	
1.9504	1.17×10^{-9}	
1.9504	1.17×10^{-9}	
1.9504	1.17×10^{-9}	
1.9504	1.17×10^{-9}	
Birnessite		
1.9655	4.18×10^{-4}	2.09×10^{-4}
1.9655	4.18×10^{-4}	
1.9066	1.03×10^{-4}	
1.9066	1.03×10^{-4}	
1.9063	1.06×10^{-4}	
1.9063	1.06×10^{-4}	
Bond angle distortion (δ^2)		
θ	$\Sigma(\theta_i - 90)^2$	δ^2
Akhtenskite		
1.9502	4.67×10^{-9}	12.32
1.9502	4.67×10^{-9}	
1.9504	1.17×10^{-9}	
1.9504	1.17×10^{-9}	
1.9504	1.17×10^{-9}	
1.9504	1.17×10^{-9}	
Birnessite		
1.9655	4.18×10^{-4}	559.41
1.9655	4.18×10^{-4}	
1.9066	1.03×10^{-4}	
1.9066	1.03×10^{-4}	
1.9063	1.06×10^{-4}	
1.9063	1.06×10^{-4}	

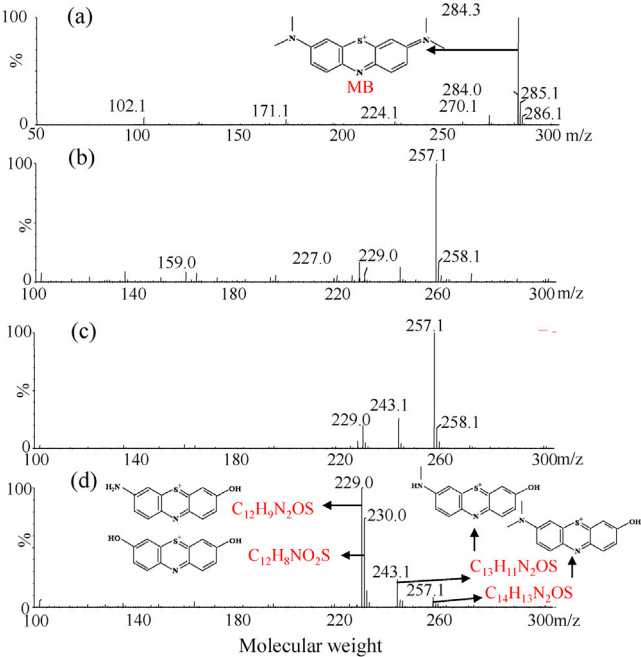
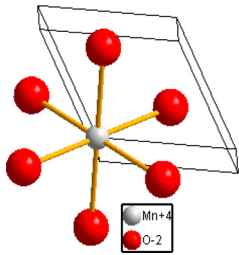
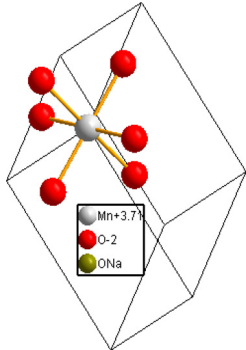
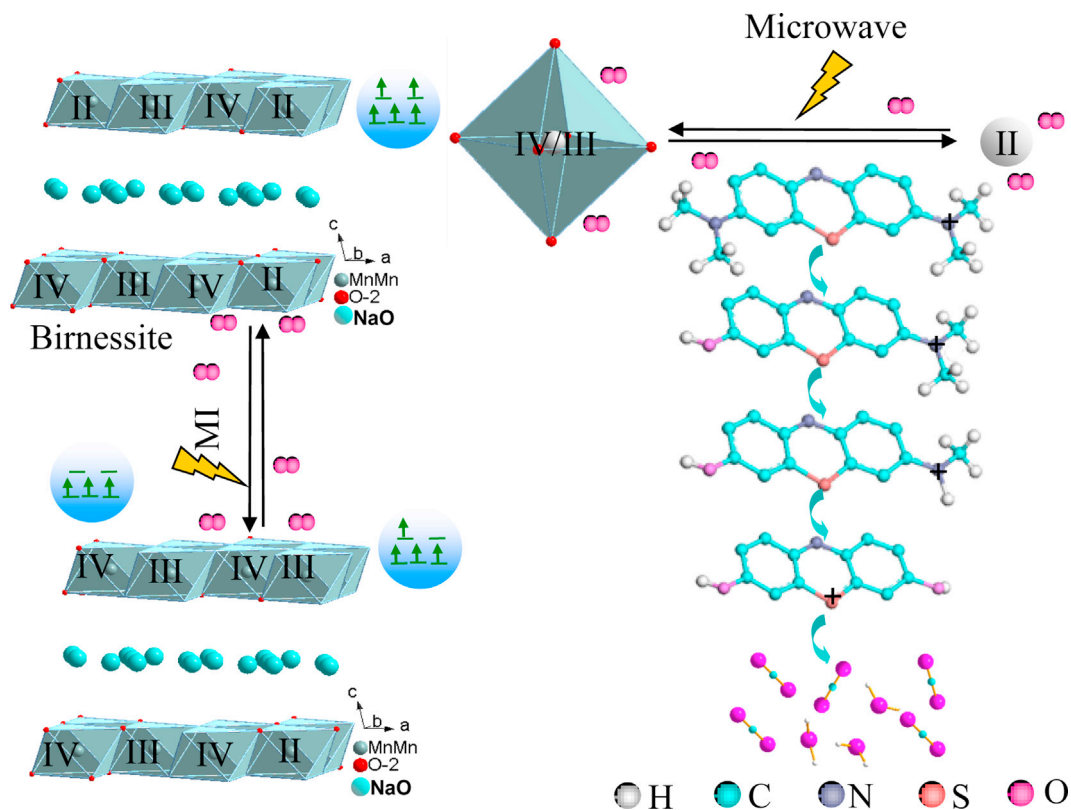


Fig. 5. LC-MS identification of MB (a) and products under MI/birnessite for 2 min (b), 10 min (c), and 60 min (d).

Table 3

Calculation of manganese oxides dipole moment.

		x	y	z
Akhtensite 	Mn	0	0	0
	O1($x - y, -1 + x, -0.5 + z$)	$-1/3$	$-2/3$	$-1/4$
	O2($x - y, x, -0.5 + z$)	$-1/3$	$1/3$	$-1/4$
	O3(x, y, z)	$1/3$	$2/3$	$1/4$
	O4($x, -1 + y, z$)	$1/3$	$-1/3$	$1/4$
	O5($1 + x - y, x, -0.5 + z$)	$2/3$	$1/3$	$-1/4$
	O6($-1 + x, -1 + y, z$)	$-2/3$	$-1/3$	$1/4$
	O	0	0	0
	Δx	0	Δy	Δz
	Dipole moment ($q \times d$)	0	0	0
Birnessite 	Mn	0	0	0
	O1($-x, -y, -z$)	-0.3765	0.003	-0.1308
	O2($0.5 - x, -0.5 - y, -z$)	0.1235	-0.497	-0.1308
	O1(x, y, z)	0.3765	-0.003	0.1308
	O4($-0.5 + x, 0.5 + y, z$)	-0.1235	0.497	0.1308
	O5($-0.5 + x, -0.5 + y, z$)	-0.1235	-0.503	0.1308
	O6($-1 + x, -1 + y, z$)	0.1235	0.503	0.1308
	O	0	0	0
	Δx	0	Δy	Δz
	Dipole moment ($q \times d$)	0	0	0

**Fig. 6.** Reaction pathway for the degradation of MB by MOs under MI.

effect of Mn(III) in octahedral sites, the lattice distortion of birnessite was more than that of akhtenskite that could also contributed to the microwave adsorption (Table 2) [37,38]. The formula for the lattice distortion calculation was given by: ($\Delta \times 10^3$ and σ^2 presenting the length and angle of distortion, respectively)

$$\Delta \times 10^3 = \frac{1}{n} \sum_{i=1}^n \left[\frac{d_i - d_m}{d_m} \right]^2 \quad (1)$$

$$\sigma^2 = \frac{1}{n-1} \sum_{i=1}^n n(\theta_i - 90^\circ)^2 \quad (2)$$

where d_i is the bond length, d_m is the average bond length, θ_i is the bond angle, and 90° is the bond angle averaged from 109.47° in tetrahedron and 120° in triangle. However, the distortion of lattice was symmetrical and the electric dipole moments of $[\text{MnO}_6]$ octahedra in akhtenskite and birnessite were both zero (Table 3).

Therefore, we predicted that spin magnetic moment of central ions played an important role in absorbing microwaves through orientation dissipation. In most MOs, central ions were in high spin states in the weak crystal field of octahedron, so lowering valence of the central ions would result in a larger spin magnetic moment [39]. XRF analysis showed that birnessite had more low valence central Mn than akhtenskite. The higher proportion of Mn(II) and Mn(III) with a larger spin magnetic moment could absorb more microwave and remove more MB, resulting in an significant increase in MB removal efficiency by birnessite. Thus, the degradation of MB was attributed to its oxidation decomposition by MOs, accompanying which Mn(IV) was reduced at the same time. Meanwhile, MI could provide a high temperature environment and accelerate the oxidation of Mn(III) or Mn(II), that were produced after MB oxidation. This latter oxidation process contributed positively to the cyclic regeneration of MOs, and thus, gradual degradation of MB to $\text{C}_{14}\text{H}_{13}\text{N}_2\text{O}_5$, $\text{C}_{13}\text{H}_{11}\text{N}_2\text{O}_5$, $\text{C}_{12}\text{H}_8\text{NO}_2\text{S}$, $\text{C}_{12}\text{H}_9\text{N}_2\text{O}_5$, and eventually to smaller molecules (Fig. 6).

4. Conclusion

This study showed that both akhtenskite and birnessite had an excellent microwave response. In the process of MI, the surface reactivity of MO increased and the removal of MB was significantly enhanced. MI was also responsible for the cyclic redox reaction of Mn and the reaction would be sustainable until MB was removed completely. MB was degraded to $\text{C}_{14}\text{H}_{13}\text{N}_2\text{O}_5$, $\text{C}_{13}\text{H}_{11}\text{N}_2\text{O}_5$, $\text{C}_{12}\text{H}_8\text{NO}_2\text{S}$, $\text{C}_{12}\text{H}_9\text{N}_2\text{O}_5$, and eventually to smaller molecules. In addition, higher MB removal was found when birnessite was used under MI in comparison to akhtenskite. As the electric dipole moment of $[\text{MnO}_6]$ octahedron in akhtenskite and birnessite were both zero and birnessite had more low valence central Mn than akhtenskite, it was predicted that a significant difference of oxidative removal ability between akhtenskite and birnessite was attributed to the larger spin magnetic moment of birnessite, which could absorb more microwaves and remove more MB than akhtenskite.

Acknowledgments

We thank M.L. Qiu and Y. Tian for their assistance in XPS and LC-MS measurements, as well as C.C. Zhao for electric dipole moment calculation. This research was jointly funded by International S&T Cooperation (No. S2014ZR0062) and Beijing Higher Education Young Elite Teacher Project (YETP0634).

References

- [1] C. Mukhopadhyay, A. Datta, Catal. Commun. 9 (2008) 2588–2592.
- [2] L. Zhang, X.-Y. Zhou, X.-J. Guo, X.-Y. Song, X.-Y. Liu, J. Mol. Catal. A Chem. 355 (2011) 31–37.
- [3] R. Carta, F. Desogus, J. Environ. Chem. Eng. 1 (2013) 1292–1300.
- [4] X.-Y. Bi, P. Wang, H. Jiang, H.-Y. Xu, S.-J. Shi, J.-L. Huang, J. Environ. Sci. 19 (2007) 1510–1515.
- [5] L. Zhang, X.-Y. Liu, X.-Y. Guo, M.-M. Su, T. Xu, X.-Y. Song, Chem. Eng. J. 173 (2011) 737–742.
- [6] Y.-M. Ju, X.-Y. Wang, J.-Q. Qiao, G.-H. Li, Y. Wu, Y. Li, X.-Y. Zhang, Z.-C. Xu, J.-Y. Qi, J.-D. Fang, D.-D. Dionysiou, J. Hazard. Mater. 263 (2013) 600–609.
- [7] T. Giannakopoulou, L. Kompotiatis, A. Kontogeorgakos, G. Kordas, J. Magn. Mater. 246 (2002) 360–365.
- [8] Q. Song, Z.-J. Zhang, J. Am. Chem. Soc. 134 (2012) 10182–10190.
- [9] B. Jang, M. Park, O.B. Chae, S. Park, Y. Kim, S.M. Oh, Y. Piao, T. Hyeon, J. Alloy. Compd. 134 (2012) 15010–15015.
- [10] O. Masala, R. Seshadri, J. Am. Chem. Soc. 127 (2005) 9354–9355.
- [11] A. Hannour, D. Vincent, F. Kahlouche, A. Tchanguoulian, S. Neveu, V. Dupuis, J. Magn. Mater. 353 (2014) 29–33.
- [12] J.-L. Zhou, L. Yu, M. Sun, S.-Y. Yang, F. Ye, J. He, Z.-F. Hao, Ind. Eng. Chem. Res. 52 (2013) 9586–9593.
- [13] L.P. Kang, M.M. Zhang, Z.H. Liua, K. Ooic, Spectrochim. Acta A 67 (2007) 864–869.
- [14] S. Turner, P. Buseck, Science 212 (1981) 1024–1027.
- [15] H.-C. Wang, H.-S. Liang, M.-B. Chang, J. Hazard. Mater. 186 (2011) 1781–1787.
- [16] C. Karamia, H. Ahmadian, M. Nouri, F. Jamshidi, H. Mohammadi, K. Ghodrati, A. farrokhi, Z. Hamidi, Catal. Commun. 27 (2012) 92–96.
- [17] J.E. Post, Proc. Natl. Acad. Sci. 96 (1999) 3447–3454.
- [18] G.-Y. Huang, L. Zhao, Y.-H. Dong, Q. Zhang, J. Hazard. Mater. 186 (2011) 128–132.
- [19] M. Oz, D.E. Lorke, G.A. Petroianu, Biochem. Pharmacol. 78 (2009) 927–932.
- [20] M.G. Shah-Khan, J. Lovely, A.C. Degnim, Am. J. Surg. 204 (2012) 798–799.
- [21] X.-H. Feng, W.-F. Tan, F. Liu, Sci. Sin. Terrae 35 (2005) 340–351.
- [22] O. Nilsen, S. Foss, H. Fjellvåg, A. Kjekshus, Thin Solid Films 468 (2004) 65–74.
- [23] C.H. Kim, Z. Akase, L.C. Zhang, A.H. Heuer, A.E. Newman, P.J. Hughes, J. Solid State Chem. 179 (2006) 753–774.
- [24] W.-T. Jiang, P.-H. Chang, Y.-S. Wang, Y. Tsai, J.S. Jean, Z.-H. Li, K. Krukowski, J. Hazard. Mater. 250–251 (2013) 362–369.
- [25] B. Lanson, V.A. Drits, E. Silvester, A. Manceau, Am. Mineral. 85 (2000) 826–838.
- [26] J.B. Kim, J.B. Dixon, C.C. Chusuei, Soil Sci. Soc. Am. J. 66 (2002) 306–315.
- [27] G.J. Racz, Plant Nutr. Fert. Sci. 1 (1994) 90–97.
- [28] J. Zhang, Q.-W. Ping, M.-H. Niu, H.-Q. Shi, N. Li, Appl. Clay Sci. 83–84 (2013) 12–16.
- [29] Y.-P. Duan, S.-H. Liu, Y.-B. Zhao, Z.-J. Ji, Physica B 405 (2010) 1826–1831.
- [30] A.D. Mani, B.R. Raju, N. Xanthopoulos, P. Ghosal, B. Sreedhar, Gh. Subrahmanyam, Chem. Eng. J. 228 (2013) 545–553.
- [31] S. Ozcan, S. Akansel, A. Ceylan, Ceram. Int. 39 (2013) 5335–5341.
- [32] A. Mills, D. Hazafy, J. Parkinson, T. Tuttle, Dyes Pigm. 88 (2011) 149–155.
- [33] M. Zaied, S. Peulon, N. Bellakhal, B. Desmazières, Appl. Catal. B Environ. 101 (2011) 441–450.
- [34] W.-H. Kuan, C.-Y. Chen, Ch.-Y. Hu, Y.-M. Tzou, Int. J. Photoenergy 2013 (2013), Article ID 916849.
- [35] H.-T. Guan, G. Chen, S.-B. Zhang, Y.-D. Wang, Mater. Chem. Phys. 124 (2010) 639–645.
- [36] J. Chen, P.-F. Tian, X.-A. Song, N. Li, J.-X. Zhou, J. Iron Steel Res. Int. 17 (2010) 13–20.
- [37] A.C. Gaillot, V.A. Dritsa, A. Manceau, B. Lanson, Microporous Mesoporous Mater. 98 (2007) 267–282.
- [38] J. Millis, P.B. Littlewood, B.I. Shraiman, Phys. Rev. Lett. 74 (1995) 5144–5147.
- [39] A.M. Haghir-Gosnet, J.P. Renard, J. Phys. D: Appl. Phys. 36 (2003) R127–R150.